Dust Aerosol Optical Centroid Height (AOCH) Over Bright Surface: First Retrieval From TROPOMI Oxygen A and B Absorption Bands

Xi Chen, Jun Wang, *Senior Member, IEEE*, Xiaoguang Xu, and Meng Zhou

***Abstract*—The vertical distribution of dust layers can influence dust transport, radiative forcing, deposition, and ultimately, surface particulate matter mass concentration. Although many dust aerosol layer height (ALH) products from passive satellite measurements have been developed, most of them are applicable on dark surfaces. Here, building on the absorbing aerosol optical centroid height (AOCH) retrieval from hyperspectral O_2 A and B absorption band measurements of the tropospheric monitoring instrument (TROPOMI) for dark target, we further develop dust AOCH retrieval over bright surfaces. Key updates include: 1) the thresholds in cloud mask tests are refined with consideration of the different spectral characteristics of bright surface reflectance; and 2) the assumption of Lambertian surface is modified to the Ross–Li bidirectional reflectance distribution function (BRDF) model to consider the angular dependence of surface reflectance. The validation against the cloud-aerosol lidar with orthogonal polarization (CALIOP) for several dust plumes over the Saharan Desert illustrates that TROPOMI AOCH has ∼1 km uncertainty and ∼0.1-km mean bias, better than ∼1 km underestimated dust-layer mean altitude (ALT) from the infrared atmospheric sounder interferometer (IASI). With this implementation of bright surfaces, our algorithm is ready for global retrieval and will be applicable for similar hyperspectral instruments in the future.**

***Index Terms*—AOCH, bright surface, dust, tropospheric monitoring instrument (TROPOMI).**

I. Introduction

AIRBORNE mineral dust usually originates from bare soil and semi-arid regions where the surfaces are bright and are lifted to different altitudes described by aerosol layer height (ALH) by winds. The model and observation analysis for several dust episodes in [1] and [2] demonstrates that the ALTs of dust plumes from different origins are distinct and determine the subsequent transport pathways. Moreover, the vertical distribution is one of the factors that significantly influences the dust radiative effect [3], [4]. In addition, the dust deposition process also depends on its ALH; for example, in the Southern Ocean, when dust particles lie in the mid- and upper-troposphere, wet deposition is the dominant removal process, while boundary layer dust is primarily removed via dry deposition [5]. The vertical distribution is also a key parameter converting columnar aerosol loading [aerosol optical depth (AOD)] into surface fine particular matter ($PM_{2.5}$) concentrations [6], indicating its significance for regional surface air pollution studies influenced by dust storm transport. Therefore, the measurements of dust vertical distribution are necessary to improve our understanding of dust impact on global climate and surface air quality.

Remote sensing is an efficient technique to detect the vertical distribution of dust particles, such as ground-based or spaceborne lidars, whose application is limited by the poor spatial coverage. Passive satellite measurements in ultraviolet (UV), visible (VIS), or near-infrared (NIR) channels have been used to retrieve columnar aerosol properties such as AOD and/or single scattering properties [7], [8], whereas until the recent decade, ALH detection using passive techniques became available. Even with only single parameter, the higher spatial resolution and coverage of passive measurements make ALH valuable in applications. Multiple passive techniques to detect dust ALH include the stereo-matching method using multiangle observations, such as from the multiangle imaging spectroradiometer (MISR), despite being limited in sensitivity to more diffuse dust plumes [9], and measurements in O_2 absorption bands in VIS-NIR, which are sensitive to the ALH of absorbing aerosols like dust. Aerosol effective height in Asia has been retrieved from the Geostationary Environment Monitoring Spectrometer (GEMS) O_2–O_2 channel (477 nm) [10]. The top height [11] or middle height [12] of a homogeneous-extinction dust layer was derived over the Atlantic Ocean (hereafter named O_2 A algorithm) by fitting hyperspectral O_2 A band (760 nm) measurements from the scanning imaging absorption spectrometer for atmospheric chartography (SCIAMACHY) or the tropospheric monitoring instrument (TROPOMI). Recently, the latest machine learning techniques have been applied in the O_2 A algorithm to make optimization more efficient [13], [14]. Combining O_2 B band (688 nm) and A band, Xu et al. [15] successfully retrieved dust aerosol optical centroid height (AOCH) over ocean from the ratio of Earth Polychromatic Imaging Camera (EPIC) measurements in O_2 absorption bands and nearby window channels (known as differential optical absorption spectroscopic, or DOAS ratio) by assuming a quasi-Gaussian extinction profile (O_2 AB

Received 27 April 2025; revised 28 July 2025; accepted 18 August 2025. Date of publication 20 August 2025; date of current version 5 September 2025. This work was supported in part by the NASA Health and Air Quality Program under Grant 80NSSC22K1047, in part by the NASA TEMPO mission, and in part by the NASA Remote Sensing Theory Program under Grant 80NSSC20K1747. *(Corresponding authors: Xi Chen; Jun Wang.)*

Xi Chen and Jun Wang are with the Department of Chemical and Biochemical Engineering, Iowa Technology Institute, The University of Iowa, Iowa City, IA 52242 USA (e-mail: xi-chen-4@uiowa.edu; jun-wang-1@uiowa.edu).

Xiaoguang Xu is with the Earth and Space Institute and GESTAR II, University of Maryland Baltimore County, Baltimore, MD 21250 USA (e-mail: xxu@umbc.edu).

Meng Zhou is with the Global Modeling and Assimilation Office, NASA Goddard Space Flight Center, Greenbelt, MD 20771 USA, also with the GESTAR II, University of Maryland Baltimore County, Baltimore, MD 21250 USA, and also with the Iowa Technology Institute, The University of Iowa, Iowa City, IA 52242 USA (e-mail: mzhou16@umbc.edu).

Digital Object Identifier 10.1109/LGRS.2025.3601046

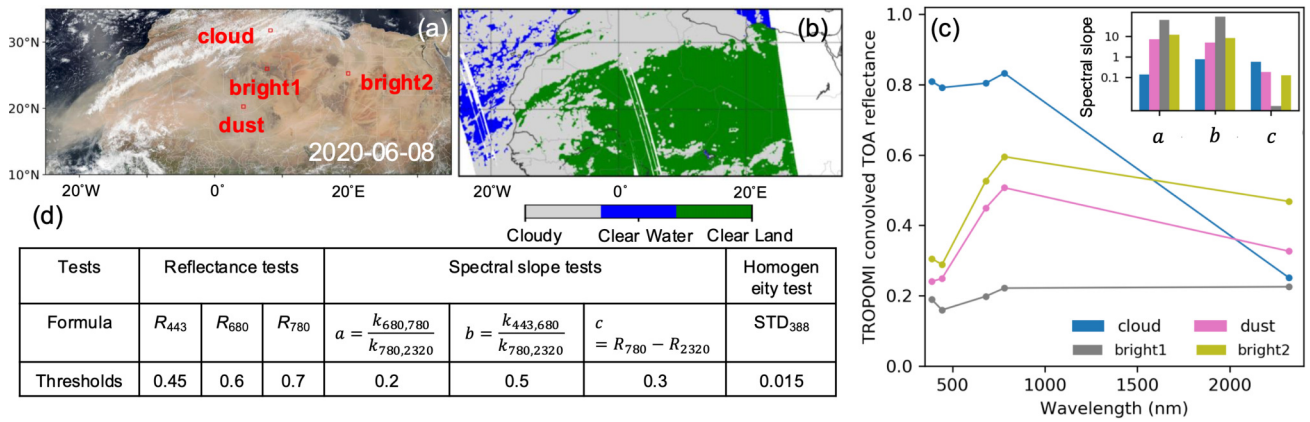

Tests	Reflectance tests			Spectral slope tests			Homogeneity test
Formula	R_{443}	R_{680}	R_{780}	$a = \frac{k_{680,780}}{k_{780,2320}}$	$b = \frac{k_{443,680}}{k_{780,2320}}$	$c = R_{780} - R_{2320}$	STD_{388}
Thresholds	0.45	0.6	0.7	0.2	0.5	0.3	0.015

Fig. 1. (a) True color image and (b) cloud classification for a Saharan Desert dust case using the spectral slope tests, reflectance tests, and spatial homogeneity test, whose thresholds are defined in (d) and (c) illustrates TROPOMI R_{λ_i} for four types of pixels highlighted in (a).

algorithm). However, most explorations above were limited to the ocean surface and the dark land. Retrieving ALH over bright surfaces, such as deserts, is more challenging due to the difficulty in isolating the dust scattering signal from the overwhelming surface contribution in VIS-NIR measurements [16], [17]. However, the use of blue band and O_2 B band, where surface reflectance is lower than at longer wavelengths, helps overcome this challenge in this study. Furthermore, there were also efforts made in thermal infrared (TIR) channels that are sensitive to large-size particles, making it feasible to retrieve dust ALH from the infrared atmospheric sounding interferometer (IASI) and atmospheric infrared sounder (AIRS) sensor [18], [19]. Unfortunately, these retrievals are less reliable over bright surfaces, due to the large uncertainty in land surface temperature and emissivity [20].

This study aims to extend our O_2 AB algorithm for dust ALH retrieval over bright surfaces. Leveraging our O_2 AB algorithm developed for EPIC [15], [17], AOCH retrieval exploration from TROPOMI has demonstrated the improvement by adding O_2 B in retrievals over dark land compared with those using only O_2 A band, due to the lower surface reflectance in the O_2 B band for most land surface types [21]. Here, we present a new development for the TROPOMI O_2 AB algorithm applied to the bright desert surface, leveraging the strengths of the Deep Blue technique [22]. Section II introduces the data used in this study. The new development applicable to bright surfaces is discussed in Section III. Section IV showcases the retrieval results and validation with lidar for dust cases over the Saharan Desert.

II. Data

A. TROPOMI L1B and L2 Data

Same as in [21], hyperspectral TROPOMI TOA radiance ($I(\lambda)$) and solar irradiance ($E_0(\lambda)$) measurements of good quality defined by quality flags are convolved using the spectral response function ($F(\lambda)$) of EPIC in six narrow bands: 388, 443, 680, 688, 764, and 780 nm, respectively, to get narrowband reflectance [see (1)]. Since shortwave infrared is not involved in EPIC, $F(\lambda)$ centered at 2320 nm is assumed as a Gaussian function of 2-nm full width at half maximum (FWHM)

$$R_{\lambda_i} = \frac{\pi \int_{\lambda_{i,1}}^{\lambda_{i,2}} F(\lambda) I(\lambda) d\lambda}{\cos(\theta_0) \int_{\lambda_{i,1}}^{\lambda_{i,2}} F(\lambda) E_0(\lambda) d\lambda} \quad (1)$$

where $\lambda_{i,1}$ and $\lambda_{i,2}$ indicate the wavelength range of $F(\lambda)$ for each narrowband λ_i, and θ_0 represents solar zenith angle. Similar to the MODIS Deep Blue algorithm, here AOD is retrieved from blue band R_{443}, where the surface reflectance is much lower than longer wavelengths, and bright surfaces like deserts and bare soil become dark [17]. The DOAS ratios, R_{688}/R_{680} and R_{764}/R_{780}, are primarily used for AOCH retrieval. To correct the mismatch in the geolocation of different spectrometers for TROPOMI, R_{λ_i} at all bands are resampled to a standard 0.05° grid using an area-weighted method [23]. The TROPOMI L2 UV aerosol index (UVAI) product is also used since AOCH retrieval is only available for pixels with UVAI > 1.0.

B. MODIS MAIAC BRDF Product

Unlike the Lambertian albedo assumption used in our previous work, the surface reflectance over bright surfaces is updated by a multiyear climatology of the semi-empirical Ross–Li bidirectional reflectance distribution function (BRDF) model derived from a 1-km MODIS MAIAC BRDF product (MCD19). In the BRDF model (2), the wavelength and geometry-dependent surface reflectance $R_s(\theta_0, \theta_v, \varphi, \lambda)$ is the sum of three kernels representing isotropic, volumetric (K_{vol}), and geometric (K_{geo}) components, respectively,

$$R_s(\theta_0, \theta_v, \varphi, \lambda) = f_{iso}(\lambda) + f_{vol}(\lambda) K_{vol}(\theta_0, \theta_v, \varphi) + f_{geo}(\lambda) K_{geo}(\theta_0, \theta_v, \varphi). \quad (2)$$

So the angular dependence of R_s is represented by K_{vol} and K_{geo} only, isolated from spectral kernel weights, f_{iso}, f_{vol}, and f_{geo}, which are provided by MCD19 at each pixel. As a result, the climatology of these kernel weights is derived from five-year products at the first seven MODIS bands and resampled to 0.05° standard grids, using the same method as TROPOMI.

C. Validation Data

For AOD validation, the version 3 level 1.5 AOD products at AERONET sites are collocated with TROPOMI retrievals spatially by averaging TROPOMI AOD falling into a 0.5° circle centered at each AERONET site. Temporally, AERONET AOD measured in a one-hour time window centered at the TROPOMI overpass time is averaged.

TABLE I

LINEAR REGRESSION COEFFICIENTS CONVERTING SURFACE REFLECTANCE FROM MODIS TO TROPOMI BANDS

MODIS bands	TROPOMI bands	Linear regression coefficients			
		0 <= NDVI < 0.1	0.1 <= NDVI < 0.4	0.4 <= NDVI < 0.6	NDVI >= 0.6
469 nm	443 nm	0.95, -2.8e-3	0.94, -4.9e-3	0.89, 5.0e-4	0.96, -3.5e-4
645 nm	680 nm	1.02, 1.6e-3	1.10, -3.7e-3	1.10, -6.6e-3	0.81, 2.3e-3
645 nm	688 nm	1.03, 2.0e-3	1.11, -1.4e-3	1.18, -8.8e-3	0.86, 5.3e-3
859 nm	764 nm	0.99, -5.7e-4	0.96, -1.5e-2	0.90, -2.3e-3	0.97, -1.4e-2
859 nm	780 nm	0.99, -6.9e-4	0.97, -1.3e-2	0.93, -3.4e-3	0.99, -1.3e-2
2130 nm	2320 nm	0.92, -1.8e-2	0.90, 1.9e-4	0.96, -1.4e-2	0.84, -8.2e-4

To quantitatively validate TROPOMI AOCH retrieval (hereafter, $AOCH_T$), an extinction weighted AOCH (hereafter, $AOCH_C$) defined as [21, eq. (6)] is derived from cloud-aerosol lidar with orthogonal polarization (CALIOP) L2 5-km aerosol extinction profiles similar to previous studies [12], [15], [17], [21]. Note that only those CALIOP footprints with total column AOD larger than 0.3 and without any cloud layers detected are considered. Rather than 532 nm, the aerosol extinction at 1064 nm is used in this study, given the less laser energy loss due to weaker aerosol extinction. Furthermore, the definition differences between $AOCH_C$ and $AOCH_T$ can cause their different values even for the same aerosol profile. Therefore, enforcing apple-to-apple comparison, $AOCH_T$ is converted into $AOCH_C$ following [24]. For each CALIOP footprint, the mean AOCH retrieval of the closest 3 × 3 TROPOMI pixels is collocated.

D. IASI Dust Product

Our TROPOMI AOCH retrievals are also cross-validated by IASI dust-layer mean altitude (ALT) retrieved by the Centre National d'Etudes Spatiales (CNES) Laboratoire de Météorologie Dynamique (LMD) algorithm here [19]. This algorithm retrieves dust AOD, ALT, and the surface temperature simultaneously from multiple window channels in IR, where dust particles are assumed to be distributed within a homogeneous layer, and ALT is defined as a height where half of the dust AOD is below (or above). IASI data from three satellites, MetOp A, B, and C, are combined as a fusion product sampled at standard 0.05° grids (same as TROPOMI) to enrich their spatial coverage given their similar morning orbit (~9:30). In the quantitative comparison, IASI ALT is also converted into equivalent $AOCH_T$(or $AOCH_C$) considering their definition difference. Given ~12-km IASI footprint, when collocating the fused IASI data with CALIOP, the closest 8 × 8 resampled IASI grids (~3 IASI footprints) are averaged. Particularly, as reported above surface, $AOCH_T$ is adjusted to be above sea level when compared with the other two.

III. ALGORITHM DESCRIPTION

The algorithm workflow of this work remains similar to that developed for dark target [21], with refinement on cloud screening and surface representation using the BRDF model. The bright surface is identified by the normalized difference vegetation index (NDVI) from MODIS MAIAC climatology.

A. Cloud Mask Tests

Different from the past study in which clouds are screened with a spatial coherence technique, the method used in this study to distinguish between clouds and bright surface relies on the distinct spectral characteristics of cloud droplets and desert surface reflectance in VIS-NIR. For instance, over bright land, the spectral slope of 780–2320 nm, $k_{780,2320}$ defined from TOA reflectance as in [21, eq. (2)], at clear sky or dust pixels is flatter than those covered by clouds [Fig. 1(c)]. Hence, similar TOA reflectance tests, spectral slope tests, and spatial homogeneity tests used in [21] are also applied to the bright surface cloud mask with empirical thresholds summarized in Fig. 1(d). Note that as a continued table of [21, Table I]

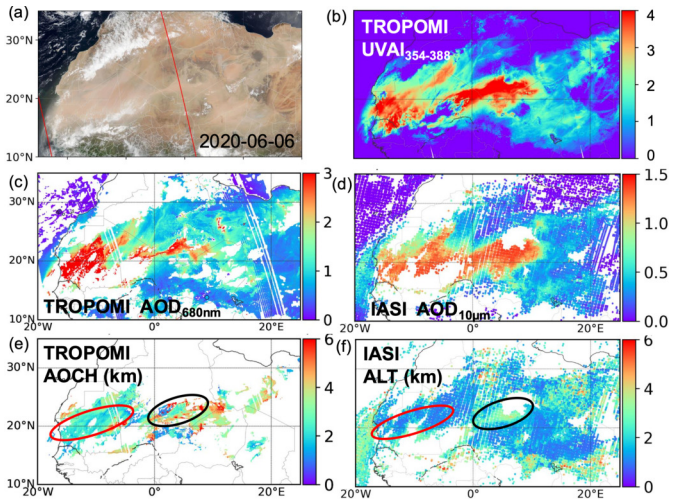

Fig. 2. Comparison of TROPOMI (c) and IASI AOD (d) and AOCH (or ALT) (e) and (f) retrievals for a Sahara dust plume on June 6, 2020, highlighted by TROPOMI UVAI (b). Red line in the true color image from VIIRS/Suomi-NPP (a) represents CALIOP track.

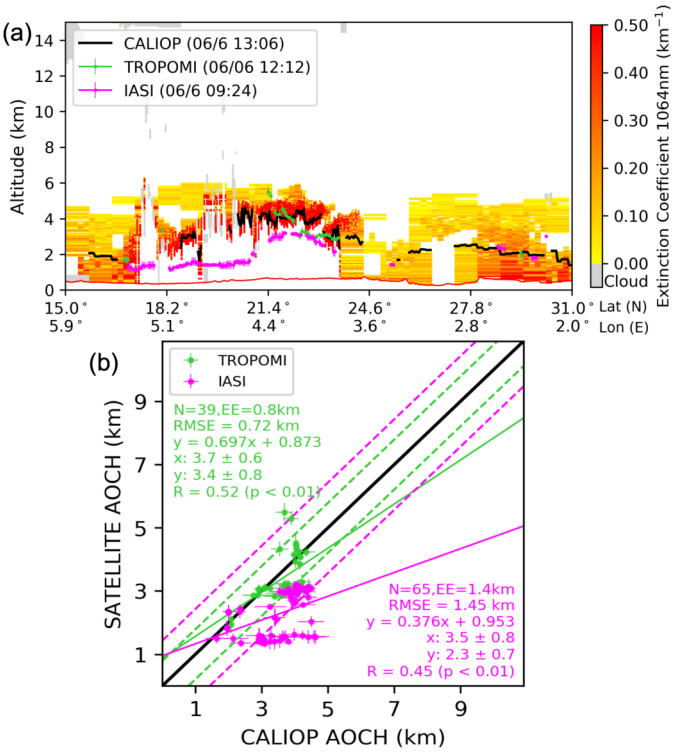

Fig. 3. Validation of AOCHT (green dots) and ALT (pink dots) against AOCHC (black line) overlapped by CALIOP extinction coefficient profiles at 1064 nm (a) and scatter plot of collocated pixels (b).

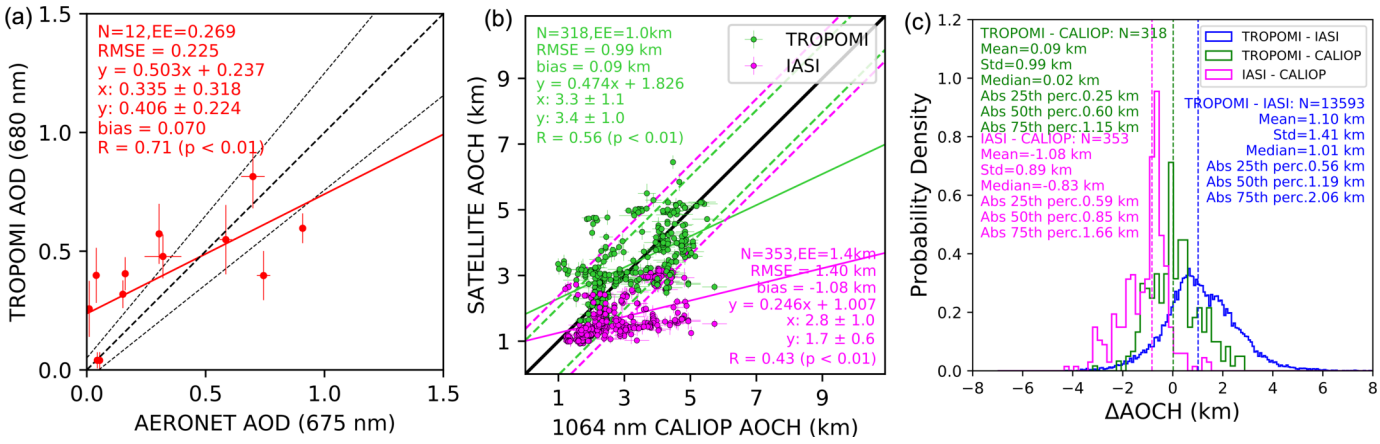

Fig. 4. Validation of (a) TROPOMI AOD against AERONET AOD and (b) $AOCH_T$ (green) or IASI (pink) ALT against $AOCH_C$ for all dust plume cases. (c) Probability histogram of AOCH differences.

for NDVI > 0.2, Fig. 1(d) is applied for the bright land of NDVI <= 0.2.

B. Surface Reflectance

With the climatology of BRDF parameters developed, the instantaneous surface reflectance (R_s) for TROPOMI geometry can be derived using the solar and viewing geometries available for each TROPOMI pixel, but in seven MODIS bands. These instantaneous R_s are fit to the TROPOMI narrowbands from the closest MODIS channels by the linear regression method based on the spectral reflectance of various surface types from the ASTER dataset [17], [21]. Here, we extend the fitting to brighter lands of NDVI <= 0.2. Ultimately, the different linear regression coefficients are applied for different surface types determined by several NDVI bins, as summarized in Table I.

IV. Retrieval Results and Validation

A. Dust Case Study

One dust plume on 6 June 2020 over the Saharan Desert is identified by the large TROPOMI UVAI (354–388 nm) values (1–4) (Fig. 2). The dust plume can be identified from both TROPOMI and IASI with high AOD [Fig. 2(c) and (d)], although their absolute values differ, considering the wavelength dependence of dust AOD. The high AOD loading of IASI and TROPOMI does not match perfectly, given their ~4 h overpass difference. Note that no further quantitative comparison of AOD between TROPOMI and IASI is conducted, considering this time lag and little information about dust microphysical properties determining dust AOD wavelength dependence. TROPOMI AOCH is only available for AOD > 0.2 and UVAI > 1.0 to ensure sufficient information content for retrieval, similar to dark surfaces [21]. From TROPOMI AOCH, the western part of the dust plume (red circle) is located at 2–3 km, while the height of the eastern part shows ~1 km higher, indicating the lifting of sand particles in the east [Fig. 2(e)]. IASI ALT also shows a similar spatial pattern, while its absolute value is ~1 km lower [Fig. 2(f)]. This spatial pattern reveals the distinction of ALH for different parts of dust plumes even in the source region, where most dust plumes originate from local soil surface or short-range transport, demonstrating the necessity of a dust ALH product with large spatial coverage for bright surfaces. The lofted eastern part of this plume is captured by CALIOP of 3–4 km $AOCH_C$ (Fig. 3), agreeing with $AOCH_T$ but ~1 km higher than ALT. The 0.52 correlation coefficient (R) between $AOCH_C$ and $AOCH_T$ indicates their consistent variation, slightly stronger than 0.45 R between $AOCH_C$ and ALT, while the root mean square error (RMSE) of 1.45 km and mean bias of −1.2 km for IASI are larger than those for TROPOMI (RMSE of 0.72 km and mean bias of −0.3 km).

One possible reason for the underestimation of IASI ALT is that IR channels show stronger sensitivity to coarse particles than VIS-NIR [25], which are more difficult to be lofted into higher altitude than finer dust particles, hence distribute more at lower altitudes. Consequently, IASI ALT is more representative of altitudes where coarse particles are located, unlike TROPOMI and CALIOP, which detect dust AOCH through VIS-NIR. Furthermore, given that IASI has a footprint twice as large as TROPOMI and CALIOP, ALT is smoother along CALIOP track with smaller error bars (standard deviation within 8 × 8 grids), while CALIOP shows more variation (larger error bars) between adjacent pixels. This contributes to the lower correlation between $AOCH_C$ and ALT. The potential cloud contamination due to the coarser resolution of IASI ALT may also explain the disagreement. The larger temporal difference between CALIOP and IASI (afternoon versus morning orbits) compared with TROPOMI could be another reason for the weaker agreement. It is also worth noting that CALIOP has a shortcoming in thick dust-layer detection, which is common in deserts. During the travel of the laser's light from space to the ground, if the dust extinction is too strong, the light cannot attenuate through the whole dust layer. Hence, aerosol extinction data could be missed below layers with strong dust extinction, such as 18°N–23°N in Fig. 3. Although these blank layers are filled by a background aerosol extinction profile of ~0.07 AOD and the CALIOP measurements at 1064 nm are used, the modification of $AOCH_C$ due to the loss of dust layer in the bottom still cannot be compensated. As a result, $AOCH_C$ can illustrate as large as 3 km differences between adjacent footprints, whereas $AOCH_T$ and ALT are smoother. This also partly explains the moderate correlation between $AOCH_C$ and $AOCH_T$ (or ALT).

B. Validation Statistics

Applying the O_2 AB algorithm developed here for another five dust cases over the Saharan Desert in June 2020,

TROPOMI AOD and AOCH retrievals are validated. Even though the collocated TROPOMI and AERONET AOD observations are not so many ($N = 12$), an R of 0.71 reveals their consistency [Fig. 4(a)]. The fitting line also indicates that the uncertainty of surface reflectance is still a crucial factor that causes the 0.225 RMSE of TROPOMI AOD. We also find that the variation of $AOCH_T$ is correlated with $AOCH_C$ of 0.56 R, with ~1-km RMSE and ~0.1-km mean bias. In contrast, IASI presents an RMSE of 1.40 and −1.08-km mean bias, revealing its underestimation. Its variation shows less correlation with CALIOP of 0.43 R. The probability density histograms of the pixel-level differences between TROPOMI, CALIOP, and IASI demonstrate that $AOCH_T$ is close to $AOCH_C$ with 0.09-km ΔAOCH on average, while IASI ALT presents a larger mean bias of −1.08 km [Fig. 4(c)]. Around 75% of TROPOMI retrievals have <1.15 km bias compared with CALIOP, smaller than the counterpart of IASI (1.66 km). Moreover, ΔAOCH among the three products all display near-normal distribution, in which the standard deviations of both $AOCH_T$ – $AOCH_C$ and ALT – $AOCH_C$ are close to 1.0 km, while a larger value of 1.41 km is found for $AOCH_T$ – ALT. In summary, TROPOMI AOCH is close to CALIOP and ~1.1 km higher than IASI.

V. Conclusion

Leveraging our published TROPOMI O_2 AB AOCH algorithm over the dark surface, this study extended its application to bright desert surfaces through further developments, which include the following.

1) Refine cloud mask tests given different characteristics of the bright surface reflectance spectrum.

2) Implement the Ross–Li BRDF model to consider the angular dependence of surface reflectance whose parameters are from MODIS MAIAC BRDF climatology.

Validation for several dust plumes over the Saharan Desert reveals that TROPOMI AOD retrievals are well correlated with AERONET and AOCH are comparable to the CALIOP extinction weighted AOCH with ~0.1-km mean bias, while IASI ALT is ~1 km underestimated with lower correlation (0.43 versus 0.56), partly due to the sensitivity of IR channels to the coarse particles at lower ALTs. Overall, TROPOMI AOD and AOCH retrievals over bright surfaces have less accuracy than those retrievals over dark land [21]. The higher surface reflectance and potentially larger uncertainty result in larger error and lower correlation of TROPOMI AOCH retrievals. Nevertheless, this ~1-km RMSE of AOCH still reveals the product's reliability in dust source regions.

References

[1] M. S. Johnson et al., "Modeling dust and soluble iron deposition to the South Atlantic Ocean," *J. Geophys. Res., Atmos.*, vol. 115, no. D15, pp. 1–13, Aug. 2010.

[2] F. Tsai, G. T.-J. Chen, T.-H. Liu, W.-D. Lin, and J.-Y. Tu, "Characterizing the transport pathways of Asian dust," *J. Geophys. Res., Atmos.*, vol. 113, no. D17, pp. 1–15, Sep. 2008.

[3] L. Zhang, Q. B. Li, Y. Gu, K. N. Liou, and B. Meland, "Dust vertical profile impact on global radiative forcing estimation using a coupled chemical-transport–radiative-transfer model," *Atmos. Chem. Phys.*, vol. 13, no. 14, pp. 7097–7114, Jul. 2013.

[4] S. Osipov, G. Stenchikov, H. Brindley, and J. Banks, "Diurnal cycle of the dust instantaneous direct radiative forcing over the Arabian Peninsula," *Atmos. Chem. Phys.*, vol. 15, no. 16, pp. 9537–9553, Aug. 2015.

[5] F. Li, P. Ginoux, and V. Ramaswamy, "Distribution, transport, and deposition of mineral dust in the Southern Ocean and Antarctica: Contribution of major sources," *J. Geophys. Res., Atmos.*, vol. 113, no. D10, pp. 1–15, May 2008.

[6] J. Wang and S. A. Christopher, "Intercomparison between satellite-derived aerosol optical thickness and $PM_{2.5}$ mass: Implications for air quality studies," *Geophys. Res. Lett.*, vol. 30, no. 21, pp. 1–4, Nov. 2003.

[7] R. C. Levy et al., "The collection 6 MODIS aerosol products over land and ocean," *Atmos. Meas. Techn.*, vol. 6, no. 11, pp. 2989–3034, Nov. 2013.

[8] O. Torres, C. Ahn, and Z. Chen, "Improvements to the OMI near-UV aerosol algorithm using A-train CALIOP and AIRS observations," *Atmos. Meas. Techn.*, vol. 6, no. 11, pp. 3257–3270, Nov. 2013.

[9] R. A. Kahn, W. Li, C. Moroney, D. J. Diner, J. V. Martonchik, and E. Fishbein, "Aerosol source plume physical characteristics from space-based multiangle imaging," *J. Geophys. Res.*, vol. 112, no. D11, pp. 1–20, 2007.

[10] S. S. Park et al., "Retrieval algorithm for aerosol effective height from the geostationary environment monitoring spectrometer (GEMS)," *Atmos. Meas. Techn.*, vol. 18, no. 10, pp. 1–40, May 2025.

[11] A. A. Kokhanovsky and V. V. Rozanov, "The determination of dust cloud altitudes from a satellite using hyperspectral measurements in the gaseous absorption band," *Int. J. Remote Sens.*, vol. 31, no. 10, pp. 2729–2744, May 2010.

[12] S. Nanda et al., "A first comparison of TROPOMI aerosol layer height (ALH) to CALIOP data," *Atmos. Meas. Techn.*, vol. 13, no. 6, pp. 3043–3059, Jun. 2020.

[13] L. Rao, J. Xu, D. S. Efremenko, D. G. Loyola, and A. Doicu, "Aerosol parameters retrieval from TROPOMI/S5P using physics-based neural networks," *IEEE J. Sel. Topics Appl. Earth Observ. Remote Sens.*, vol. 15, pp. 6473–6484, 2022.

[14] S. Nanda et al., "A neural network radiative transfer model approach applied to the tropospheric monitoring instrument aerosol height algorithm," *Atmos. Meas. Techn.*, vol. 12, no. 12, pp. 6619–6634, Dec. 2019.

[15] X. Xu et al., "Passive remote sensing of altitude and optical depth of dust plumes using the oxygen A and B bands: First results from EPIC/DSCOVR at Lagrange-1 point," *Geophys. Res. Lett.*, vol. 44, no. 14, pp. 7544–7554, Jul. 2017.

[16] X. Chen, X. Xu, J. Wang, and D. J. Diner, "Can multi-angular polarimetric measurements in the oxygen—A and B bands improve the retrieval of aerosol vertical distribution?," *J. Quant. Spectrosc. Radiat. Transf.*, vol. 270, Aug. 2021, Art. no. 107679.

[17] X. Xu et al., "Detecting layer height of smoke aerosols over vegetated land and water surfaces via oxygen absorption bands: Hourly results from EPIC/DSCOVR in deep space," *Atmos. Meas. Techn.*, vol. 12, no. 6, pp. 3269–3288, Jun. 2019.

[18] C. Pierangelo, A. Chédin, S. Heilliette, N. Jacquinet-Husson, and R. Armante, "Dust altitude and infrared optical depth from AIRS," *Atmos. Chem. Phys.*, vol. 4, no. 7, pp. 1813–1822, Sep. 2004.

[19] S. Peyridieu et al., "Characterisation of dust aerosols in the infrared from IASI and comparison with PARASOL, MODIS, MISR, CALIOP, and AERONET observations," *Atmos. Chem. Phys.*, vol. 13, no. 12, pp. 6065–6082, Jun. 2013.

[20] J. Zheng et al., "Thermal infrared dust optical depth and coarse-mode effective diameter over oceans retrieved from collocated MODIS and CALIOP observations," *Atmos. Chem. Phys.*, vol. 23, no. 14, pp. 8271–8304, Jul. 2023.

[21] X. Chen et al., "First retrieval of absorbing aerosol height over dark target using TROPOMI oxygen B band: Algorithm development and application for surface particulate matter estimates," *Remote Sens. Environ.*, vol. 265, Nov. 2021, Art. no. 112674.

[22] N. C. Hsu et al., "Enhanced deep blue aerosol retrieval algorithm: The second generation," *J. Geophys. Res.*, vol. 118, no. 16, pp. 9296–9315, 2013.

[23] J. Wang et al., "Detecting nighttime fire combustion phase by hybrid application of visible and infrared radiation from Suomi NPP VIIRS," *Remote Sens. Environ.*, vol. 237, Feb. 2020, Art. no. 111466.

[24] H. Kim et al., "Aerosol layer height (ALH) retrievals from oxygen absorption bands: Intercomparison and validation among different satellite platforms, GEMS, EPIC, and TROPOMI," *Atmos. Meas. Techn.*, vol. 18, no. 2, pp. 327–349, Jan. 2025.

[25] X. Xu et al., "Sense size-dependent dust loading and emission from space using reflected solar and infrared spectral measurements: An observation system simulation experiment," *J. Geophys. Res., Atmos.*, vol. 122, no. 15, pp. 8233–8254, Aug. 2017.